ECE540 Project 1: Double-slit Interference using FDTD with PML and PMC

Yi-Chia Tsai (NetID: yichiat2)[a)]
Department of Electrical and Computer Engineering, University of Illinois at Urbana-Champaign, Urbana, Illinois 61801, USA and Micro and Nanotechnology Laboratory, University of Illinois at Urbana-Champaign, Urbana, Illinois 61801, USA

(Dated: 9 October 2019)

The Finite-Difference Time-Domain (FDTD) methods have been implemented under the Yee-grid algorithm to study the double-slit interference problems. Perfectly matched layers (PML) have been implemented to simulate infinite space with zero reflection; while, the boundary condition between vacuum and the perfect magnetic conductor (PMC) has been carefully maintained so that electromagnetic (EM) waves are able to propagate through micro-scale slits and reproduce interference patterns. The objective of the project is to understand the fundamental physics and numerical analysis of EM waves.

Keywords: Maxwell's Equations, EM-Field, FDTD, Double-slit Interference, PML, PMC

I. INTRODUCTION

Electromagnetic (EM) waves are the oscillation of electric fields and magnetic fields, traveling at the speed of light. By modulating the oscillation frequency of EM waves, different wavelength of EM waves can be achieved ranging from radio waves, infra-red, visible light, ultraviolet light, X-rays, and gamma-rays, which are widely studied for communications, detection, illumination, sterilization...etc. Basically, EM wave problems are universal in our daily life. To improve the aforementioned applications, it is an important task to study EM waves.

Maxwell's equations[1] have governed the classical electromagnetism and photonics for more than sesquicentennial. Although it has been used to study the fundamental physics of EM waves under certain approximations, assumptions, and idealization, not until recently, it can be applied for realistic applications. Thanks to the increased computational capability, Finite-Difference Time-Domain (FDTD) techniques with Yee-grid algorithm[2] are proposed to solve the Maxwell's equations numerically. The FDTD algorithm discretizes the continuous time-dependent partial differential equations into a set of subtractions in discrete grids; while, Yee-grid method simplifies the boundary problems and avoids the corner singularity of EM fields by translating the magnetic grid relative to the electric grid with 1/2 of each lattice vector. FDTD with Yee-grid offers multiple advantages that the analytical solutions cannot achieve. For example, the propagation of EM waves in nonuniform medium or the medium with asymmetric shape can be studied. However, the standard FDTD cannot deal with the EM wave problems in an infinitely-extended space, which is essential for long-range communications. To simulate EM waves propagating in an unbounded space, perfect matched layers (PML), lossy medium that are able to absorb the incident EM waves and result in minimal reflection, are appended at the boundary of simulation domains. As a consequence, FDTD algorithm implemented with Yee-grid and PML techniques is able to study a variety of EM wave problems in an infinitely large space.

In this project, EM waves propagating through perfect magnetic conductor (PMC) with double slits are investigated to study the wave interference behavior in two dimensions, where the EM waves are generated by an infinitely long current. Time-domain Maxwell's equations are solved numerically using FDTD algorithms with Yee-grid and PML.

II. COMPUTATIONAL DOMAIN AND METHODS

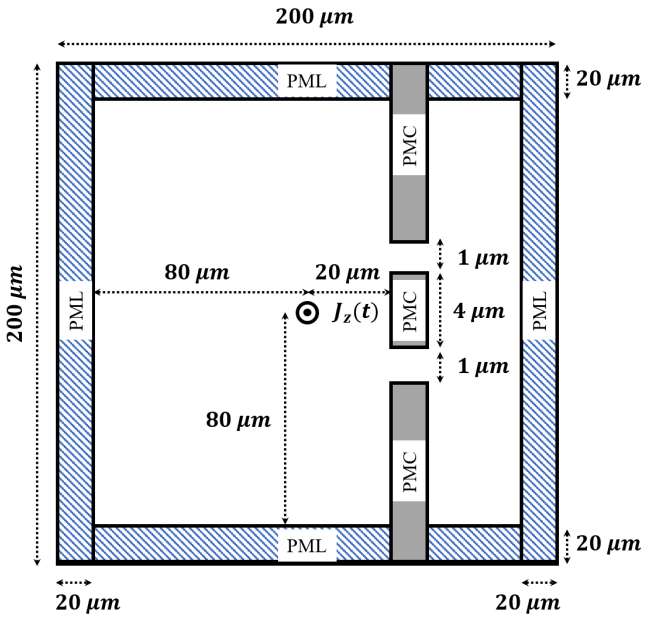

FIG. 1: Schematic illustration and geometrical parameters of the simulation domain, PML, and PMC.

[a)]Address: Innovative COmpound semiconductoR (ICOR) Laboratory, Urbana, Illinois 61801, USA. Electronic mail: yichiat2@illinois.edu. Telephone: +1 (217) 974-5750. URL: `http://icorlab.ece.illinois.edu`.

A. Discretization of Modified Maxwell's Equations

Maxwell's equations in 2D can be simplified as transverse magnetic (TM) and transverse electric (TE) modes. In this project, the TM mode is considered, where the z-component of magnetic fields and the x, y-component of electric fields are zero ($H_z = 0, E_x = 0, E_y = 0$). As a result, two Faraday's equations and one Maxwell–Ampere equation left:

$$\begin{aligned} \frac{\partial E_z}{\partial y} &= -\mu \frac{\partial H_x}{\partial t} \\ \frac{\partial E_z}{\partial x} &= \mu \frac{\partial H_y}{\partial t} \\ \frac{\partial H_y}{\partial x} - \frac{\partial H_x}{\partial y} &= \varepsilon \frac{\partial E_z}{\partial t} + \sigma E_z + J_z. \end{aligned} \tag{1}$$

However, the equations have not been generalized for the lossy medium in the PML. Therefore, the coordinate-stretched curl operator is applied, which expressed as:

$$\nabla_s = \hat{x} \frac{1}{1 - j\frac{\sigma_x}{\omega\varepsilon}} \frac{\partial}{\partial x} + \hat{y} \frac{1}{1 - j\frac{\sigma_y}{\omega\varepsilon}} \frac{\partial}{\partial y}, \tag{2}$$

where σ_x and σ_y are the conductivity of PML along x and y directions, respectively. Consequently, by assuming lossless medium and source-free condition in the computation domains, Eq. 1 can be modified and formulated as:

$$\begin{aligned} \frac{\partial}{\partial y}\left(E_{z,x} + E_{z,y}\right) &= -\mu \frac{\partial H_x}{\partial t} - \frac{\sigma_y \mu}{\varepsilon} H_x \\ \frac{\partial}{\partial x}\left(E_{z,x} + E_{z,y}\right) &= \mu \frac{\partial H_y}{\partial t} + \frac{\sigma_x \mu}{\varepsilon} H_y \\ \varepsilon \frac{\partial E_{z,x}}{\partial t} + \sigma_x E_{z,x} &= \frac{\partial H_y}{\partial x} \\ \varepsilon \frac{\partial E_{z,y}}{\partial t} + \sigma_y E_{z,y} &= -\frac{\partial H_x}{\partial y} \end{aligned}, \tag{3}$$

where $E_z = E_{z,x} + E_{z,y}$. Since the current source does not locate inside the PML, the calculation of electric field, i.e. the last two modified equations in Eq. 3, with the consideration of current source degenerates into the last equation in Eq. 1, where $\sigma_x = \sigma_y = 0$. Next, Eq. 3 can be discretized on the computational domains using E-centered Yee-grid algorithm. The time-stepping equations including the contribution of current source and the implementation of PML are

$$\begin{aligned} H_x^{n+\frac{1}{2}}(i, j+\frac{1}{2}) &= \frac{1}{\beta_y(i, j+\frac{1}{2})}\{\alpha_y(i, j+\frac{1}{2}) H_x^{n-\frac{1}{2}}(i, j+\frac{1}{2}) - \frac{\varepsilon}{\mu\Delta y}\left[E_z^n(i, j+1) - E_z^n(i, j)\right]\} \\ H_y^{n+\frac{1}{2}}(i+\frac{1}{2}, j) &= \frac{1}{\beta_x(i+\frac{1}{2}, j)}\{\alpha_x(i+\frac{1}{2}, j) H_y^{n-\frac{1}{2}}(i+\frac{1}{2}, j) + \frac{\varepsilon}{\mu\Delta x}\left[E_z^n(i+1, j) - E_z^n(i, j)\right]\} \\ E_{z,x}^{n+1}(i, j) &= \frac{1}{\beta_x(i, j)}\{\alpha_x(i, j) E_{z,x}^n(i, j) + \frac{1}{\Delta x}\left[H_y^{n+\frac{1}{2}}(i+\frac{1}{2}, j) - H_y^{n+\frac{1}{2}}(i-\frac{1}{2}, j)\right]\} \\ E_{z,y}^{n+1}(i, j) &= \frac{1}{\beta_y(i, j)}\{\alpha_y(i, j) E_{z,y}^n(i, j) - \frac{1}{\Delta y}\left[H_x^{n+\frac{1}{2}}(i, j+\frac{1}{2}) - H_x^{n+\frac{1}{2}}(i, j-\frac{1}{2})\right]\} \\ E_z^{n+1}(i, j) &= E_{z,x}^{n+1}(i, j) + E_{z,y}^{n+1}(i, j) - \frac{\Delta t}{\varepsilon} J_z^{n+\frac{1}{2}}(i, j), \end{aligned} \tag{4}$$

Notably, $\alpha_{x,y,z} = \frac{\varepsilon}{\Delta t} - \frac{\sigma_{x,y,z}}{2}$ and $\beta_{x,y,z} = \frac{\varepsilon}{\Delta t} + \frac{\sigma_{x,y,z}}{2}$. A steep change of conductivity at the boundary between vacuum and PML leads to high reflection rate. Therefore, a gradient change of conductivity is adopted, which is expressed as:

$$\sigma_{x,y} = -\frac{m+1}{2\eta L} ln|R(0)| \left(\frac{l}{L}\right)^m, \tag{5}$$

where $\eta = 120\pi\Omega$, l, $L = 20\mu m$, and $R(0)$ are the wave impedance, the distance between points inside PML and the boundary of the simulation domain, the thickness of PML, and the reflectance of EM wave incident normal to the PML, respectively. $m = 3$ is the parameter to control the steepness of conductivity change in the PML. For the given structural parameter, the maximum conductivity is 6721.6 Sm^{-1} at the edge of simulation domain.

B. PMC Boundary Condition

Similar to the perfect electric layers (PEC), the surface of PMC can support surface magnetic current and charge. However, the surface magnetic current and charge are imaginary components, which equal to zero. Therefore, the tangential component of magnetic fields are zero on the surface of PMC. Benefiting from the Yee-grid approach, the H_x and H_y are tangent to the PMC surface in 2D TM mode formalism. As a consequence, $H_x = 0$ and $H_y = 0$ are carefully maintained on the surface of PMC. Technically, a 2D flag-map is constructed to mark the

boundary of PMC. In the 2D flag-map, the grid points on the boundary normal to x, y, and both directions are marked as "1", "–1", and "2", which imply $H_y = 0$, $H_x = 0$, and $H_x = H_y = 0$, respectively. During the iteration of magnetic fields, the 2D flag-map is used in $if/else$ conditional statements to locate the grid points where the boundary conditions should be considered.

C. Simulation Domain and Current Source

The final step is to define the simulation domain and geometry of PML and PMC quantitatively. Fig. 1 shows the geometrical parameters of the simulation domain, PML, and PMC. Notably, according to the stability analysis of central-difference approach, the time step (Δt) is set as:

$$\Delta t = \frac{1}{c\sqrt{(\Delta x)^{-2} + (\Delta y)^{-2}}}. \tag{6}$$

Assuming $\Delta x = \Delta y = h$, the time step inherently yields a numerical dispersion of

$$\frac{\pi^2 h^2}{24\lambda^2}\left(1 + \cos(4\phi)\right), \tag{7}$$

where λ and ϕ are the wavelength and the incident angle of EM waves,respectively. Table I summarizes the geometrical and discretization parameters for FDTD simulations. Since the numerical dispersion depends on the frequency or the wavelength of EM waves, the current source is simulated using modulated Gaussian pulse to test the PML functionality and reflection error; while, for the investigation of double-slit interference patterns, single-frequency source is used as a continuous current source.

The modulated Gaussian current pulse is formulated by

$$J_z(t) = Ae^{-\frac{1}{2}\left(\frac{t_0 - t}{\tau_p}\right)^2} \times \sin\left(\omega_0\left(t_0 - t\right)\right) \tag{8}$$

TABLE I: Geometrical and discretization parameters for FDTD simulations.

Parameter	Value
Length of simulation domain	200 μm
Width of simulation domain	200 μm
Δx	1 μm
Δy	1 μm
Δt	2.358×10^{-15} s
m	3
σ_{max}	6721.6 Sm^{-1}
Thickness of PML	20 μm
Thickness of PMC	10 μm
Width of PMC slit	1 μm
Width of PMC barrier	4 μm
Distance between J_z and PMC	20 μm

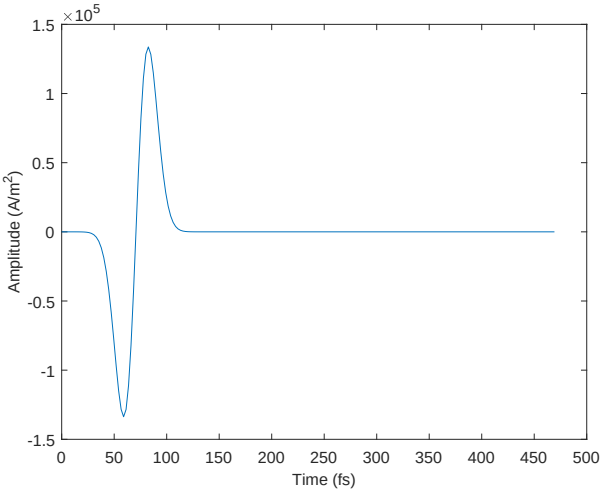

(a) The modulated Gaussian current pulse.

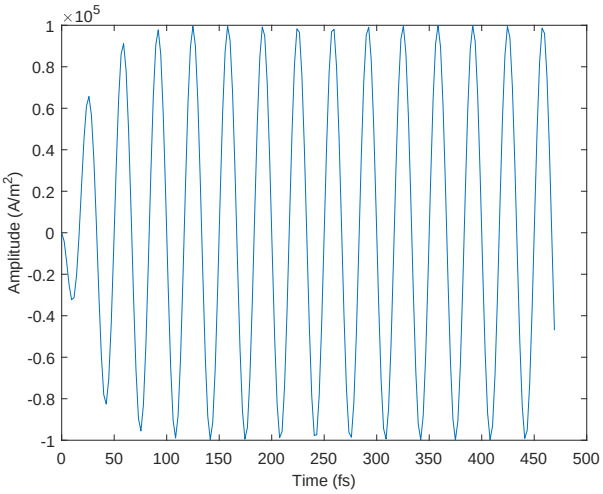

(b) The single-frequency current source.

FIG. 2: Two types of the applied current sources

and the single-frequency current source is formulated by

$$J_z(t) = A\left[e^{\left(-\frac{t}{\tau_p}\right)} - 1\right] \times \sin\left(\omega_0 t\right), \tag{9}$$

where A, t_0, τ_p, and ω_0 are amplitude, reference time, dispersion parameter, and modulation angular frequency, respectively. Table II lists the quantitative parameters used to generate the modulated Gaussian current pulse and single-frequency current source, where Figs. 2a and 2b demonstrate the signal in time domain, respectively.

III. RESULTS AND DISCUSSION

A. Numerical v.s. Analytical Approaches

The radiation generated by time-harmonic, uniform, and infinitely long line current, in free space can be solved

TABLE II: Parameters for generating modulated Gaussian current pulse and single-frequency current source.

Parameter	Modulated Gaussian Pulse	Single-Frequency Source
Amplitude (A) (A/m^2)	10^6	10^5
Reference time (t_0) (s)	7.074×10^{-14} (=30 Δt)	0
Dispersion parameter (τ_p) (s)	1.179×10^{-14} (=5 Δt)	2.358×10^{-14} (=10 Δt)
Modulation angular frequency (ω_0) (rad/s)	1.885×10^{13}	1.885×10^{14}

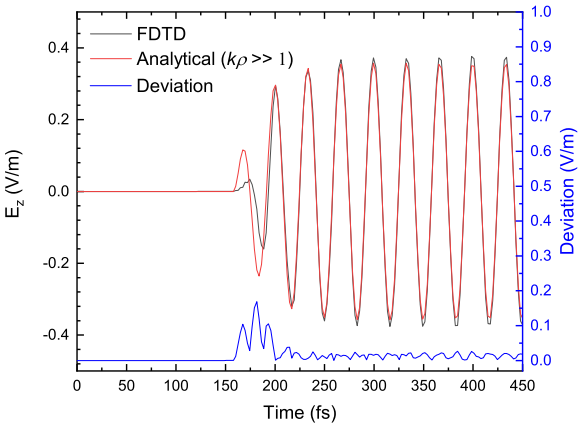

FIG. 3: Comparison of FDTD and analytical (far-field) E_z solutions at $\rho = 50$ μm as t = 0–450 fs, where $k\rho = 31.43 >> 1$.

analytically through Helmholtz equation. The E_z solution can be expressed in form of *Hankel* functions $H_0^2(k\rho)$ expressed as:

$$E_z = -\frac{k^2 I(t)}{4\omega\varepsilon} H_0^2(k\rho) = -\frac{\eta k I(t)}{4} H_0^2(k\rho), \tag{10}$$

where η and $k = 6.286 \times 10^5$ m^{-1} are the wave impedance and wavevector based on the parameters of single-frequency source listed in Tab. II. respectively. In the far-field zone where $k\rho >> 1$, the *Hankel* function can be approximated by

$$H_0^2(k\rho) \approx \sqrt{\frac{2}{\pi k\rho}} e^{-j\left(k\rho - \frac{\pi}{4}\right)}, \tag{11}$$

which can be used to approximate Eq. 10 and gives an analytical expression of E_z in the far-field zone:

$$E_z \approx -\eta I(t) \sqrt{\frac{k}{8\pi\rho}} e^{-j\left(k\rho - \frac{\pi}{4}\right)}. \tag{12}$$

Figure 3 compares the E_z calculated by FDTD and Eq. 12, where $\rho = 50$ μm, t = 0–450 fs, and $k\rho = 31.43 >> 1$. The left y-axis shows the E_z; while, the right y-axis shows the magnitude of deviation between the FDTD and analytical solutions. The E_z calculated by FDTD travels 167 fs to reach the reference point; while, Eq. 12 gives the steady-state solutions. Therefore, in order to compare the results, the analytical solutions are shifted 167 fs backwardly so that FDTD and analytical solutions are synchronized. When t < 200 fs, the transient response is not captured by the analytical solution, therefore, the analytical solution overestimates the E_z, resulting in a larger deviation of ∼0.10 V/m. However, when t > 200 fs, the FDTD results are close to the steady-state solutions, which yield a smaller deviation of ∼0.017 V/m. The deviation is caused by multiple reasons: (a) the shape of current source (square in the FDTD, cylindrical in the analytical solution), (b) the approximation of $H_0^2(k\rho)$, (c) discretization and reflection errors, which are going to be explored in the following sections.

B. Discretization Error

The discretization error originates from the finite-difference method, which approximates derivatives in real space by subtractions in discrete elements. To demonstrate the discretization error, the modulated Gaussian current pulse is applied, where the grid point (30 μm away from the current source) is sampled as a reference point. Fig. 4 demonstrates the evolution of E_z as time goes from 59 fs to 507 fs. First of all, the modulated Gaussian pulse propagates isotropically, indicating the stability of time step. Secondly, the modulated Gaussian pulse reaches the reference point at t = 177 fs, which takes about 107 fs for the propagation, and lead to $E_z = -0.258$ V/m. Since the current pulse drops significantly below 10^{-8} A/m^2 and 10^{-19} A/m^2 after t > 160 fs and t > 195 fs, respectively, due to the exponential nature of the modulated Gaussian pulse. Therefore, the reference point is expected to follow the same declination rate. However, the simulation domain is defined in discrete space, the finite size of each grid point make it difficult to follow up the steep change in signal, known as discretization error. Therefore, the E_z at t = 295, 413, and 460 fs are -2.959×10^{-4}, -2.633×10^{-5}, and -1.414×10^{-5} V/m,respectively. Thirdly, the pulse reaches the PML at t > 413 fs and is significantly absorbed, indicating the functionality of PML. However, as t > 460 fs, the reflection error reflected by the PML reaches the reference point and increases the $E_z = -3.417 \times 10^{-4}$. At this time frame, both discretization and reflection error add

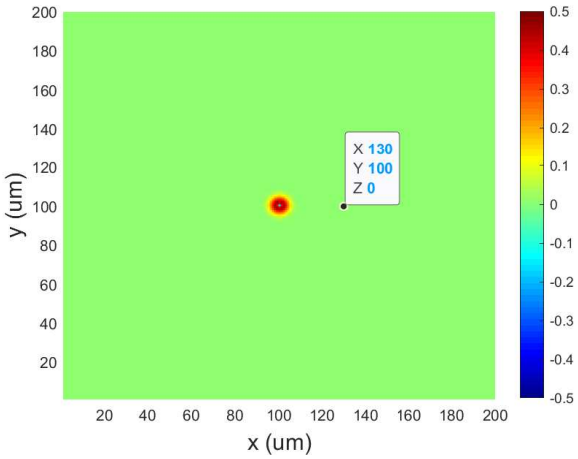

(a) E_z (V/m) at t = 59 fs.

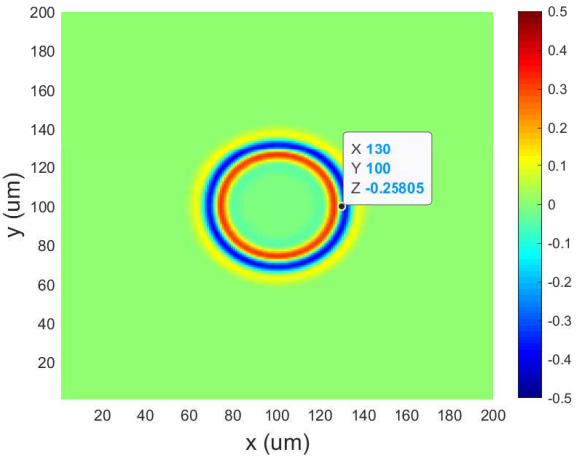

(b) E_z (V/m) at t = 177 fs.

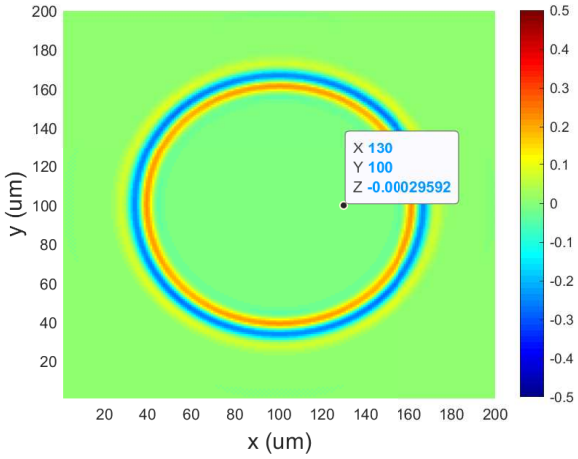

(c) E_z (V/m) at t = 295 fs.

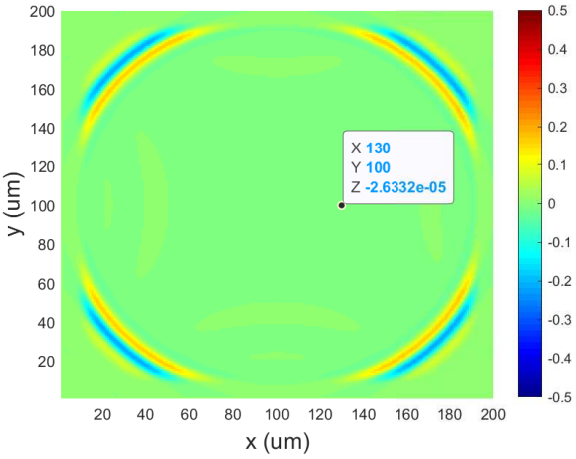

(d) E_z (V/m) at t = 413 fs.

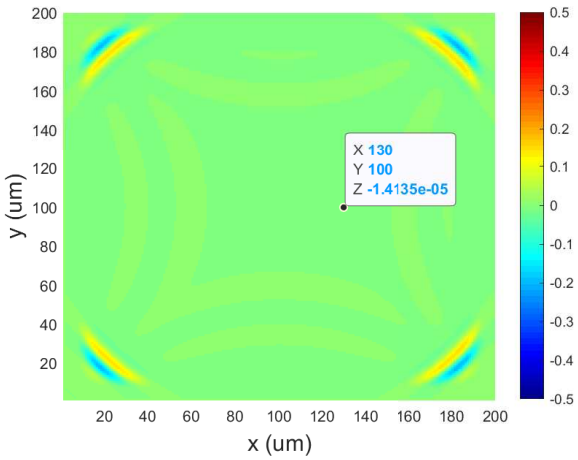

(e) E_z (V/m) at t = 460 fs.

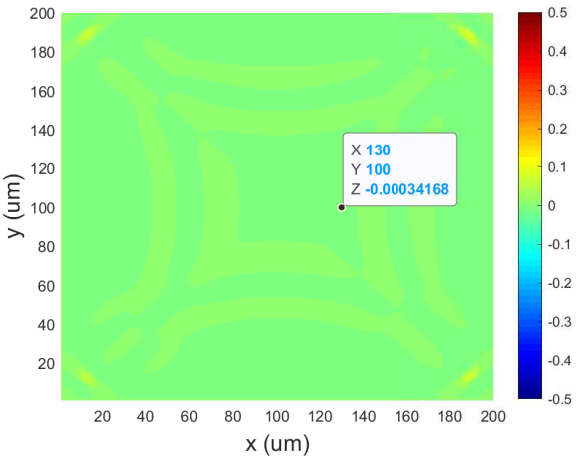

(f) E_z (V/m) at t = 507 fs.

FIG. 4: Evolution of E_z when the time goes from 59 fs to 507 fs.

tp together and contribute to the reference point. The next session will measure the reflection error. In short, the discretization error, according to the geometrical and source settings listed in Tabs. I and II, is about 1×10^{-5} V/m.

C. PML Reflection Error

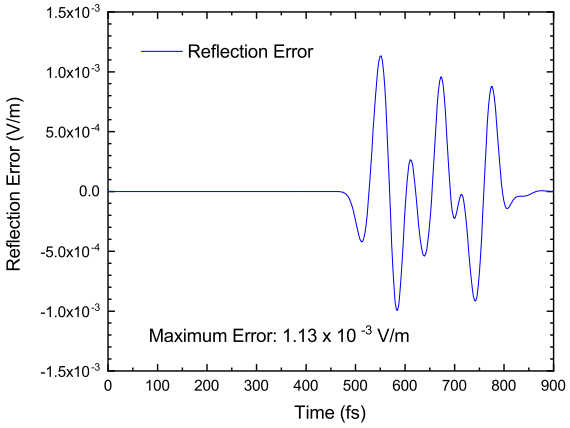

FIG. 5: Time-dependent reflection error when t spans from 0 to 900 fs.

The reflection error originates from the steep change in conductivity and the absorbing capability in different wavelengths and incident angles. To isolate the reflection error from the dicretization error, a larger simulation domain, which doubles the size in x and y directions (400 μm $\times$ 400 μm), is constructed. Notably, in order to maintain the same discretization error, the size of each grid points (Δx and Δy) and time step (Δt) should be kept the same as the original case listed in Tab. 1. Similar to Sec. III B, the modulated Gaussian current pulse is placed in the middle of the enlarged simulation domain; while, the grid point, which is 30 μm away from the source is sampled as a reference point. To study the reflection error, proper time frames have to be selected appropriately so that the reflected EM waves have reached the sampling point in the smaller simulation domain (200 μm $\times$ 200 μm) but not in the larger simulation domain (400 μm $\times$ 400 μm). Figure 5 demonstrates the time-dependent reflection error on the sampling point. The refection error is calculate by subtracting the E_z of the sampling point in the 400 μm $\times$ 400 μm case from the 200 μm $\times$ 200 μm case. There is zero reflection error when t $<$ 460 fs because the reflected E_z has not reached the sampling point in the 200 μm $\times$ 200 μm case. Although the discretization error still exists in both cases, they are identical. As a result, the subtraction cancels the discretization error leaving the pure reflection error. When 460 $<$ t, the reflected E_z reaches the sampling point in the 200 μm $\times$ 200 μm case; while, the E_z in the 400 μm $\times$ 400 μm case is still propagating toward the PML or the reflected E_z has not yet reached the sampling point. In these times frames, the magnitude of reflection error is highly dependent on the waveform and intensity of the original modulated Gaussian current pulse, where the oscillation of reflection error is the result of the constructive and destructive interference among the E_z reflected by four boundaries. In short, the maximum reflection error is 1.13×10^{-3} V/m.

D. Double-Slit Interference

Double-slit experiment is essential to study the interference nature of EM waves. Therefore, the continuous single-frequency current source is applied to generate stable oscillation source with single frequency. Fig. 6 demonstrates the evolution of E_z propagating through the double-slit made by PMC as t goes from 80 to 399 fs. At t = 80 fs, the E_z has not yet reaches the PMC, therefore, a clear isotropic waveform is observed. When t = 151 fs, the E_z is propagating through the double slits. It worth noting that the E_z reflected by the PMC boundary interferes with the original source and form constructive and destructive interference patterns at $x < 120$ μm region. When t = 226 fs, the double slits behave as two E_z sources and interfere with each other, merging into single waveform. Finally, when t = 399 fs, the EM waves reach the PML. Again, the waves are properly absorbed by the PML, therefore, there is no sign of interference between the PML-reflected E_z and the source-generated E_z through the entire simulation domain. The boundary condition between vacuum and PMC has been maintained perfectly on both sides since there is no sign of EM-wave penetrations even if t = 800 fs and longer. Additionally, in order to make the slits with 1 grid width work properly, the boundary condition in the slits are examined grid by grid. Fig. 7(a) demonstrates the interference pattern along the x direction sliced from Fig. 6(d) at $y = 100$ μm. It shows that there are able 5 periods of E_z propagate through the PMC before entering the PML. The wavelength of E_z is 10 μm, which is identical to the source frequency, indicating the consistency of wavelength and frequency throughout the entire simulation domain. Fig. 7(b) demonstrates the interference pattern along the y direction sliced from Fig. 6d at $x =$ 159 μm, which is 29 μm away from the PMC. The interference pattern is caused by the path difference when the E_z from two slits. Destructive patterns are formed when the E_z from two slits have the opposite phase, on the contrary, constructive patterns are formed when the E_z from two slits have the same phase.

IV. CONCLUSIONS

In conclusion, Finite-Difference Time-Domain method has been implemented in MATLAB R2019a; while, perfectly matched layer (PML) has been incorporated

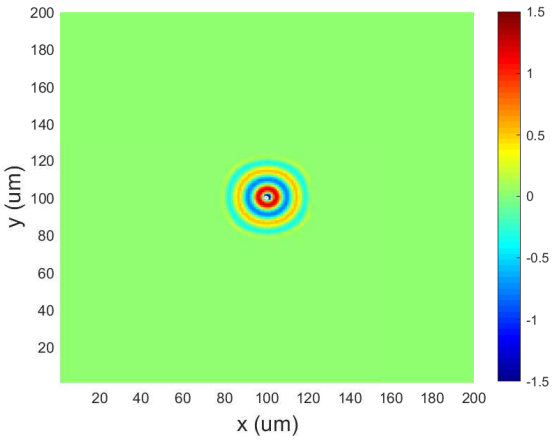

(a) E_z (V/m) at t = 80 fs.

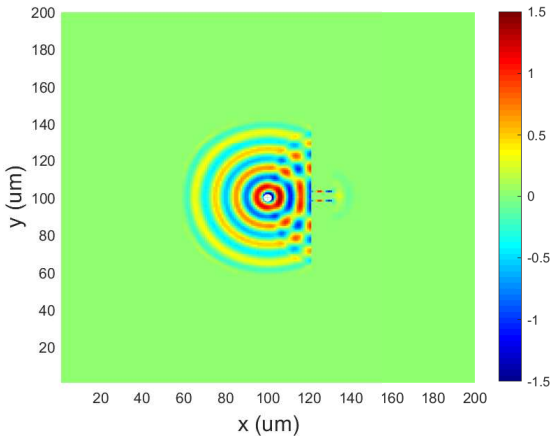

(b) E_z (V/m) at t = 151 fs.

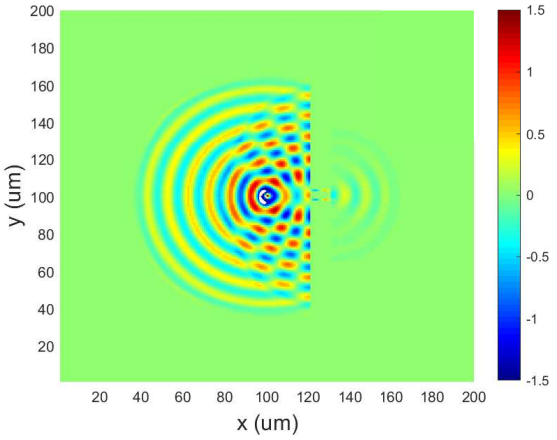

(c) E_z (V/m) at t = 226 fs.

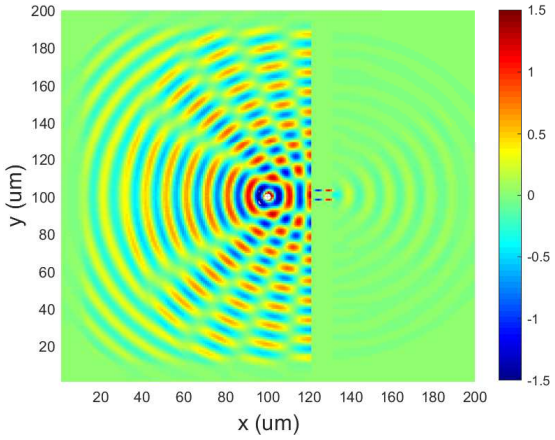

(d) E_z (V/m) at t = 399 fs.

FIG. 6: Evolution of E_z propagating through the double-slit made by PMC when t goes from 80 fs to 399 fs.

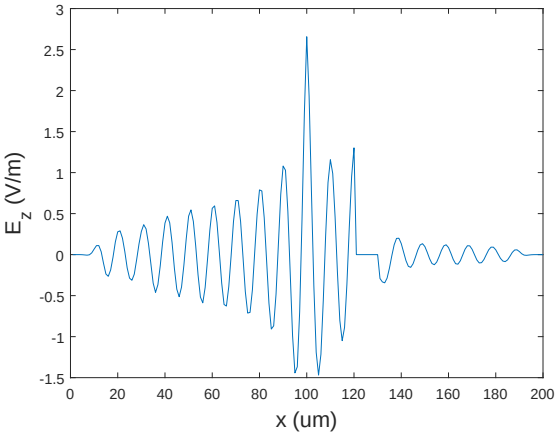

(a)

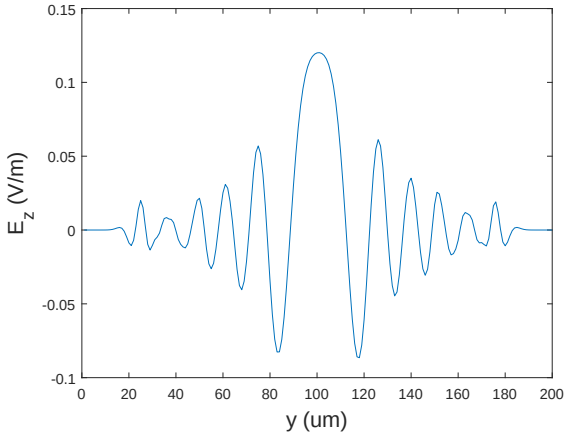

(b)

FIG. 7: E_z interference pattern along the (a) x and (b) y directions taken at $y = 100$ μm and $x = 159$ μm, respectively, while t = 399 fs for both cases.

to simulate electromagnetic wave problems in the infinitely-extended space. Under Yee-grid formalism, the boundary condition of TM mode can be easily implemented; while, the corner sigularity can be prevented. The accuracy of FDTD has been studied by comparing with analytical solutions, quantifying the magnitude of discretization and reflection errors. Based on the well-analyzed algorithms and codes, the algorithms are applied to reproduce and study the double-slit experiments, where the perfect magnetic conductor is considered as the barrier layer. Eventually, the numerical FDTD tool can be used to study the transient response of more complicated structures, such as rings and asteroids, to the EM waves.

ACKNOWLEDGEMENT

This work is supported by the National Science Foundation Faculty Early Career Development (CAREER) Program under award number NSF-ECCS-16-52871. The authors acknowledge the computational resources allocated by Extreme Science and Engineering Discovery Environment (XSEDE) with No. TG-DMR180050 and TG-DMR180075.

[1] J. C. Maxwell, Philosophical Transactions of the Royal Society of London **155**, 459 (1865).
[2] Kane Yee, IEEE Transactions on Antennas and Propagation **14**, 302 (1966).

Appendix A: Source Code Implemented in MATLAB R2019a